Journal of Solid State Chemistry 181 (2008) 2250–2259

Contents lists available at ScienceDirect

Journal of Solid State Chemistry

journal homepage: www.elsevier.com/locate/jssc

The role of the coordination defect: A new structural description of four fluorite-related sesquioxide minerals, bixbyite (Mn_2O_3), braunite (Mn_7SiO_{12}), braunite II ($CaMn_{14}SiO_{24}$), parwelite ($Mn_{10}Sb_2As_2Si_2O_{24}$), and their structural relationships

D.J.M. Bevan [a,*], R.L. Martin [b]

[a] School of Chemistry, Physics and Earth Sciences, The Flinders University of South Australia, Bedford Park, South Australia, Australia
[b] School of Chemistry, Monash University, Clayton, Victoria, Australia

ARTICLE INFO

Article history:
Received 9 February 2008
Received in revised form
24 April 2008
Accepted 28 April 2008
Available online 17 May 2008

Keywords:
Anion-deficient fluorite-related structures
Sesquioxides
Bixbyite
Braunite
Braunite II
Parwelite
Coordination defect

ABSTRACT

The anion-deficient, fluorite-related structures of the manganese-based minerals bixbyite (Mn_2O_3), braunite (Mn_7SiO_{12}), braunite II ($CaMn_{14}SiO_{24}$) and parwelite ($Mn_{10}Sb_2As_2Si_2O_{24}$) are reinterpreted in terms of the coordination defect (CD) theory to gain new insights into their structural interrelationships. CDs are extended, octahedral defects centred by an anion vacancy and including its immediate atomic environment: it is represented as $\square M_4O_6$, where the symbol $\square$ is the anion vacancy. The bixbyite *motif* is a CD dimer (two edge-sharing octahedra), and this *motif* repeats, by further edge-sharing, around the 2-fold screw axes of the cubic structure. These same dimers are present in each of the other structures, but the presence of Si^{4+} in braunite and braunite II, together with that of other foreign cations such as As^{5+} and Sb^{5+} in parwelite, leads to different juxtapositions of these *motifs*. Moreover, the structure of braunite, $Mn^{2+}(Mn^{3+})_6SiO_{12}$, reflects the clustering of 12 Mn^{3+}-centred octahedra (MnO_6) around a central SiO_4 tetrahedron to generate a structure for the $[(Mn^{3+})_6SiO_{12}]^{2-}$ anion which is almost identical to that of the well-known cuboctahedral structure of the PO_4-centred heteropolytungstate anion, $[(W^{6+})_{12}PO_{40}]^{3-}$. The structure of braunite II, $[Ca(Mn^{3+})_{14}SiO_{24}]$, is simply an intergrowth of slabs of bixbyite- and braunite-type structures, linked by the CaO_8 cubes of the latter.

Our various analyses of the reported structure of parwelite in terms of the only possible vacancy assignment have led to some apparent anomalies. We report briefly on these, and have decided to seek confirmation of the reported structure as a consequence.

Despite the increasing complexity of these structures, there are clear and defining relationships in the distribution of CDs. The assumption of a close relationship to the fluorite parent in all these structures is based on the observation that the cation sub-lattices are essentially face-centred cubic, with the anions in the tetrahedral sites, so there is little variation from this between one structure and another. The cation contents, however, are very different in the four structures discussed here — a single cation species in bixbyite, two in the braunites and four in parwelite. This factor, and the topology of the CD arrangements, are structure-determining and confirm the close relationships between these four minerals.

1. Introduction

The fluorite (CaF_2) structure is parent to a large number of binary transition metal oxides and oxide-fluorides, as well as to many other minerals with more complex chemistry. These compounds include the dioxides of elements such as Ce, Tb, Pr, Th, U and Pu in which the M^{4+} cations of a face-centred cubic (*fcc*) array lie at the centres of cubes of eight O^{2-} anions, whereas the anions lie at the centres of regular tetrahedra of four M^{4+} cations, forming two subsets, *A* and *B*, of interpenetrating *fcc* arrays related by mirror symmetry. The list also includes a great many binary oxides, $MO_{2\pm x}$, based on the dioxides of the rare-earth metals Ce, Pr, Tb, and U, many ternary systems MO_2–M_2O_3 (M = cation) such as CeO_2–R_2O_3 (R = rare earth other than Ce) [1–3], as well as the ordered oxides in the ternary CaO–HfO_2 system [4].

It is generally accepted that such compounds, both binary and ternary, can range in overall composition between $MX_{1.5}$ and

* Corresponding author.
E-mail addresses: Ray.Martin@sci.monash.edu.au, judge.bevan@flinders.edu.au (D.J.M. Bevan).

0022-4596/$ - see front matter © 2008 Elsevier Inc. All rights reserved.
doi:10.1016/j.jssc.2008.04.046

$MX_{2.33}$ (X = anion: most commonly oxygen and/or fluorine) and contain a multitude of different elements (mainly cations). In anion-deficient compounds, the multiplicity of oxidation states exhibited by the cations can be accommodated by the creation of a balancing number of vacant oxygen sites in the derivative structures, the essential constants being the nominally *fcc* array of the cations, and anion occupancy of tetrahedral sites.

In the middle of the last century, many such fluorite-related systems were broadly classed as "non-stoichiometric compounds" [5], "defect solids" or "solid solutions", and most early treatments of these followed the classical, thermodynamics-based, point-defect theory (vacancies or interstitials) first developed by Schottky and Wagner [6]. Subsequent developments in both thermodynamic [7] and crystallographic studies [8–12] led to the discovery of numerous ordered superstructure phases within the broad composition ranges of what had previously been described as "non-stoichiometric solids", e.g. UY_6O_{12} [9], $Zr_4Sc_3O_{12}$ and $Zr_5Sc_2O_{13}$ [10], $Zr_3Yb_4O_{12}$ [11], and several phases in the $CaO–HfO_2$ system [12].

It is also well known that an ordered series of rare-earth oxides occurs between R_7O_{12} and RO_2 (R = Ce, Pr, Tb), where the oxidation states III and IV occur in various ratios. These fluorite-related "superstructures", to which must be added the *C*-type sesquioxide, R_2O_3, conform to the generic formula R_nO_{2n-2m}, (R_4O_6: $n=4$, $m=1$: R_7O_{12}; $n=7$, $m=1$: R_9O_{16}; $n=9$, $m=1$: $R_{40}O_{72}$; $n=40$, $m=4$: $R_{11}O_{20}$; $n=11$, $m=1$: $R_{24}O_{44}$; $n=24$, $m=2$), each with $2m$ vacant oxygen sites, designated as □ [13,14].

Electron and X-ray diffraction studies, combined with density data, had all confirmed that, for each superstructure, the cation lattice remained intact and essentially *fcc*, with a mixture of cationic oxidation states III and IV occurring in well-defined but differing ratios, and that the resulting charge imbalance was accommodated entirely by the creation of the requisite number of untenanted tetrahedral oxygen sites in the anion sub-lattice: $2Pr^{4+}+O^{2-} = 2Pr^{3+}+□$. Thus, for example, $Pr_{40}O_{72}$ is more precisely designated as $Pr_{40}O_{72}□_8$ with $16Pr^{3+}$ and $24Pr^{4+}$ cations. However, the small contribution made by the oxygen atoms to the overall X-ray intensity data in the early studies posed a problem in structure analysis for the direct location of the vacant anion sites, with early attempts involving only the refinement of the anion occupancies [4].

The first detailed structures for the various members of the praseodymium (and terbium) oxide series were proposed by Von Dreele et al. [15–19] on the basis of exploring all possible model structures by Rietveld analysis of powder neutron diffraction data — if the experimental data fitted those calculated for a model, it was assumed to be the correct structure.

The structures of the rare-earth homologues have been described further by Bevan and Martin [20], subsequent to earlier descriptions by Hoskins and Martin [21,22], in terms of Martin's original "coordination defect" (CD) model, described below. In this paper we focus on applying CD theory to explore the structures and illuminate subtle interrelationships between four naturally-occurring, fluorite-related, sesquioxide minerals, *viz.* bixbyite (Mn_2O_3), braunite (Mn_7SiO_{12}), braunite II ($CaMn_{14}SiO_{24}$) and parwelite ($Mn_{10}Sb_2As_2Si_2O_{24}$). In particular, we have attempted to answer the challenge posed by Moore and Araki [23] exactly 30 years ago: *"Of all known inorganic compounds, these complex oxides are perhaps the most resistant to formal structural description and classification and for this reason there exists no adequate treatment in the standard pedagogical treatises."*

2. The CD theory

The CD theory has considerably enhanced our understanding of such complex superstructure phases. In 1974, Martin [24] proposed that the anion vacancies were not simply isolated point defects randomly distributed throughout the fluorite lattice, but rather that each vacancy was strongly coordinated by its nearest neighbours, four cations and six anions, to generate an octahedral structural entity of considerable thermodynamic and structural stability. In particular, it was argued that the octahedral topology of the resulting CD was a key structure-determining factor in all anion-deficient fluorite phases.

The concept of the CD is based on an oxygen-centred, polyhedral description of the fluorite structure, *viz.* OM_4 tetrahedra sharing edges to fill space. In these anion-deficient phases, oxygen atoms are missing within an essentially fixed *fcc* cation lattice, and the CD, a new kind of extended defect (*cf.* shear planes [25]), is here defined as an octahedron of OM_4 tetrahedra sharing corners to create an empty tetrahedron ($□M_4$) or, alternatively, an empty tetrahedron, ($□M_4$), sharing all six edges with OM_4 tetrahedra: this is shown in Figs. 1a and b for the types *A* and *B* subsets, and formulated as $□M_4(OM_4)_6$. The $□M_4$ tetrahedron is virtually "included" (in the geometrical sense) within the $(OM_4)_6$ octahedron, as shown in Fig. 1c, where only the $□O_6$ octahedron is drawn.

Indeed, there are advantages, as we shall see later, in representing the full CD just as $□M_4O_6$. We justify this by arguing that, for an isolated CD within a fluorite matrix, the perturbation on the lattice resulting from the missing O atom (the vacancy, □) does not extend significantly beyond the oxygen atoms of the $□O_6$ octahedron. Moreover, an inevitable consequence of creating a vacant oxygen site is an *expansion* of the tetrahedron of cations encapsulating the vacancy. Such a phenomenon can provide a useful probe for locating anion vacancies in an oxygen-deficient fluorite lattice, and has been clearly observed in numerous earlier structural studies (*cf.* [4] and references therein) as well as those reported here.

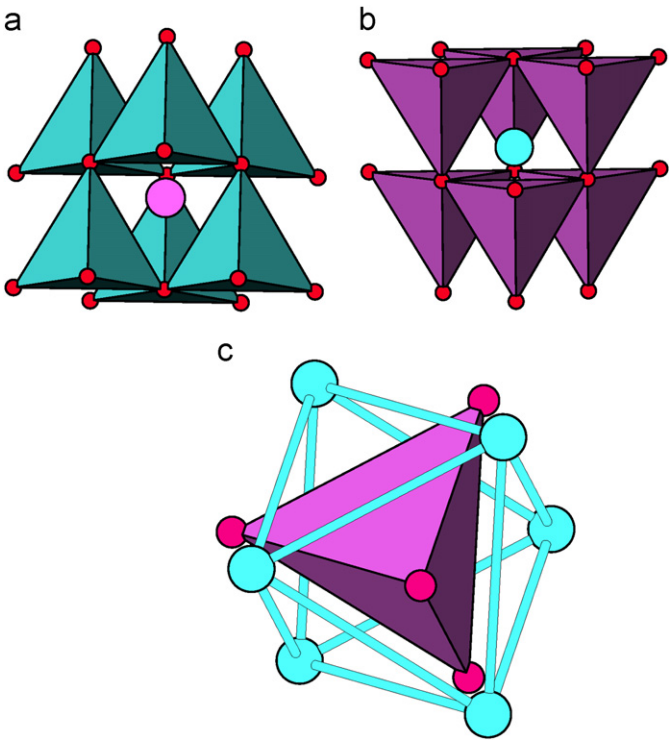

Fig. 1. (a) The central, "virtual" atom (pink: type B) represents the vacancy (□) at the centre of the so-called B-type CD. (b) The central, "virtual" atom (light blue: type A) represents the vacancy (□) at the centre of the so-called A-type CD. (c) Another representation of a CD: a $□M_4$ tetrahedron (type B) "included" within a $□O_6$ octahedron (type A).

In shorthand, the CD is designated (*mutatis mutandis*) either as $\square M_4$ or $\square O_6$. The first designation emphasises the tetrahedral, metallic CD core; the second, the octahedron of the peripheral oxygen atoms or OM_4 tetrahedra. Incorporated into the fluorite-type structure, and therefore taking account of the sharing of all tetrahedral edges such that every M atom is common to 8 tetrahedra, the CD composition becomes $\square M_{4/8}(OM_{4/8})_6$ or $M_7O_{12}\square_2$, which is indeed the composition of the most stable phase of the rare-earth series [7].

Since the anion sub-lattice of the fluorite structure consists of two interpenetrating *fcc* arrays, there are two subsets for the OM_4 and $\square M_4$ tetrahedra, and the two corresponding CDs (*A* & *B*: Figs. 1a and b). It should be noted that the octahedron of six OM_4 tetrahedra sharing corners are all of one subset, while the encapsulated $\square M_4$ tetrahedron is of the other subset. It is sometimes convenient to define the CD simply in terms of the subset of this $\square M_4$ tetrahedron (see below).

Bevan and Martin [20] recognised two types of the shortest ($\frac{1}{2}\langle 111\rangle_F$: $\frac{1}{2}\sqrt{3}a$, where a is the cell edge of fluorite) CD linkages in the intermediate rare-earth oxide series: these are the so-called "anti-phase" CD linkages between *A*- and *B*-type CDs involving edge-sharing of the peripheral OM_4 tetrahedra, which are shown in Figs. 2a and b, the second involving corner-sharing of two $\square M_4$ tetrahedra with a common cation.

They have pointed out (as did Hoskins and Martin [21,26]) that in the rhombohedral phase M_7O_{12} ($MO_{1.714}$) the packing of the CDs is as close as is possible while still retaining individual CD integrity. This follows from the derived CD formula (see above), so that every atom in the unit cell is part of a CD.

Interestingly, compounds with the formula $In_{4+x}Sn_{3-2x}Sb_xO_{12}$ (M_7O_{12}), having the same rhombohedral structure, form excellent transparent conducting layers with wide applications in the field of optoelectronics [27]. However, we are concerned here only with structural principles, not applications.

It follows, therefore, that a necessary consequence of any reduction of the O/*M* ratio in these oxides below 12/7 is that the individual integrity of each CD can no longer be retained, and it is no accident that phase studies of various MO_2–M_2O_3 "solid-solution" systems (mainly rare-earths), both pseudo-binary and ternary [1,3], have shown a diphasic region between this composition (M_7O_{12}) and the onset of a sesquioxide (M_8O_{12})-related phase at a lower O/*M* ratio.

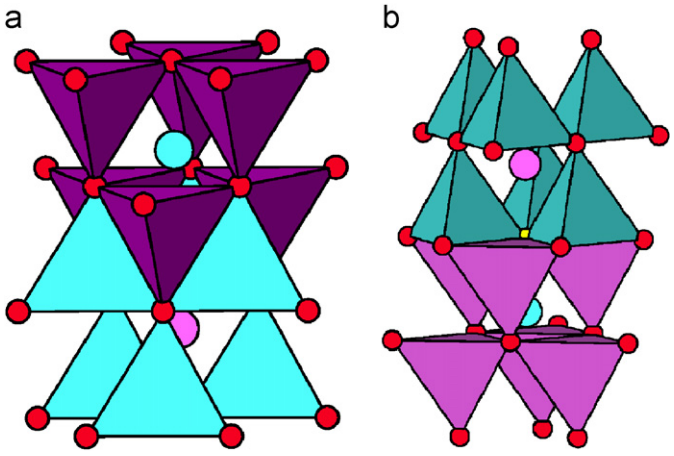

Fig. 2. (a) One of the two shortest-possible *anti-phase* CD linkages between *complete* CDs of types A and B – *viz.* $\frac{1}{2}\langle 111\rangle$F. The two types of $\square M_4$ tetrahedra are separated by an empty M_6 octahedron created by the way in which the three OM_4 tetrahedra from each CD share edges. (b) The other of the two shortest-possible *anti-phase* CD linkages between complete CDs of types A and B – *viz.* $\frac{1}{2}\langle 111\rangle$F. The two types of $\square M_4$ tetrahedra are linked through a common *M* vertex (shown in yellow) resulting from the way in which the three OM_4 tetrahedra from each CD share edges.

The composition of the reduced end-member of the above generic series is the sesquioxide $MO_{1.50}$: (M_4O_6: $n=4$, $m=1$). The sesquioxides of the rare-earth elements occur as one or more of three structure types, known generally as *A*, *B* or *C*. The first of these is hexagonal, the second monoclinic and the third cubic, and much has been written about them [13]. The present paper is focussed solely on the *C*-type sesquioxide structure, which occurs not only for yttria and the heavier rare-earths, including Pr_2O_3 and Tb_2O_3, but also for a large number of naturally-occurring minerals. In particular, we analyse below the structures of the *C*-type-related minerals bixbyite, the two braunites and parwelite to explore to what extent the integrity of the individual CD may be compromised, and then to reassess its value in predicting, or at least rationalising, the structures of these reduced phases and their interrelationships.

3. Mineral chemistry

Bixbyite, the two braunites and parwelite are manganese-based minerals found in the rich Långban-type deposits in Bergslagen, Sweden [28]. These ore deposits exhibit great species diversity due to the presence of numerous foreign cations not usually found in association with each other, such as Sb^{5+}, As^{5+} and Si^{4+}. The mineral bixbyite, a slightly impure Mn_2O_3 containing a small amount of Fe, is cubic and isostructural with the *C*-type rare-earth sesquioxides, although its parent, pure α-Mn_2O_3, is slightly distorted to orthorhombic. Among the sesquioxides of the trivalent transition metal cations, Ti, V, Cr, Mn and Fe, manganese is unique, being the only one that does not have the corundum-type structure, almost certainly due to the considerable Jahn–Teller distortion associated with its high-spin $3d^4$ configuration.

Braunite [$Mn^{2+}(Mn^{3+})_6SiO_{12}$], unlike bixbyite, contains silica and is tetragonal with its *c*-axis being double that of bixbyite. However, De Villiers [29] has pointed out that the cation positions in braunite correspond closely to those of bixbyite, and that the structures are closely related. Moore and Araki [30] have confirmed this. De Villiers [29] also suggested that silica substitution arises from the charge-balancing replacement, $2Mn^{3+} = Si^{4+}+Mn^{2+}$, in a hypothetical bixbyite parent, Mn_8O_{12}.

De Villiers and Herbstein [31] earlier had described a second, naturally-occurring phase, braunite II, with half the silica content but double the *c*-axis of braunite, i.e. four times that of bixbyite: De Villiers has subsequently determined the structure [32].

Parwelite [$(Mn^{2+})_{10}(Sb^{5+})_2(As^{5+})_2\ Si_2O_{24}$] is a highly complex oxide and has been described by Moore and Araki [23] as "*perhaps the most complicated fluorite derivative structure to-date*". The structure is complicated by the considerable distortions introduced through the presence of the highly-charged foreign cations. We propose here that, in addition to silica substitution for manganese(III) arising from the charge-balancing replacement, $2Mn^{3+} = Si^{4+}+Mn^{2+}$, the presence of arsenic and antimony in parwelite involves the further charge-balancing replacements, $3Mn^{3+} = Sb^{5+}+2Mn^{2+}$ and $3Mn^{3+} = As^{5+}+2Mn^{2+}$; i.e. the overall substitution in a hypothetical bixbyite parent is $8Mn^{3+} = 5Mn^{2+}+Si^{4+}+Sb^{5+}+As^{5+}$.

4. Crystal chemistry

The *C*-type structure for sesquioxides is well known: it is cubic, space group $Ia\bar{3}$, with a cell-edge doubled with respect to the *fcc* fluorite cell. Pauling and Shapell [33] once described it as fluorite with 25% of the anion sites vacant in an ordered manner. All that

such a statement should signify, however, is that the type-*C* cation lattice, like that of all fluorite-related structures, is nominally *fcc*, within which the anions occupy the tetrahedral sites. And, as Moore and Araki [23] have pointed out, the same is true of the multi-cation minerals braunite, braunite II and parwelite, all of which are themselves related to bixbyite.

4.1. Bixbyite

In the real structure of bixbyite [34] the cations occupy the 8*a* site of $Ia\bar{3}$ at 0,0,0 etc. and the 24*d* site at $x,0,\frac{1}{4}$, etc., with $x = 0.2855$. The anions occupy the general 48*e* site, *x,y,z* (0.1293, 0.1471, −0.0835) while the 16*c* site, *x,x,x*, is unoccupied, and is the site of the "anion vacancies", with $x = 0.125$. The cell formula is $M_{32}O_{48}\square_{16}$. While location of the anion vacancies can be achieved by identifying those oxygen sites enclosed by an expanded M_4 tetrahedron (*vide supra*), we have employed here the simpler confirmation of this identification by superimposing the ideal fluorite oxygen sites of the unit cell on a drawing of the actual structure and then matching the observed oxygen atom sites to those of fluorite: the missing match then locates the vacancy site. In this structure, the cations are, of course, identical, although this is not true for their environments since they occupy two distinct crystallographic sets. Thus, the $Mn(1)O_6$ octahedron is quite regular, with all six Mn(1)–O bonds of length 2.003 Å, while the $Mn(2)O_6$ polyhedron is highly distorted: Mn–O distances are 2 at 1.898 Å, 2 at 1.986 Å and 2 at 2.242 Å: it can be described as a twisted trigonal prism, consistent with Jahn-Teller distortion arising from the asymmetric $3d^4$ configuration of Mn (III).

There is only one general set for the anions so all are equivalent, as are the vacancies in site 16*c*, but we have distinguished the two vacancy subsets in what follows. The vacancy separation within each subset is now just $\frac{1}{2}\langle 110\rangle_F$: $\frac{1}{2}\sqrt{2}a$, where *a* is the cell edge of fluorite). These linkages (three per vacancy) are shown in Fig. 3 near the [001] projection, demonstrating infinite, interpenetrating, 3D networks of the linked vacancies of each subset.

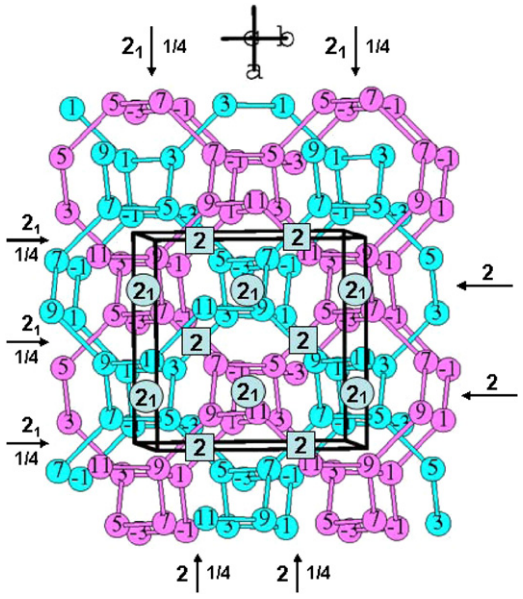

Fig. 3. The bixbyite vacancy networks projected near [001]. Some 2- and 2_1-axes are indicated. *Each set* of vacancies (light blue and pink respectively) forms an infinite, 3D network of $\frac{1}{2}\langle 110\rangle_F$ linkages spiralling around these axes. *z*-parameters for each vacancy are given in eighths, indicating the same chirality for the spirals within each set, but opposite chirality between sets. These *independent* networks simply interpenetrate.

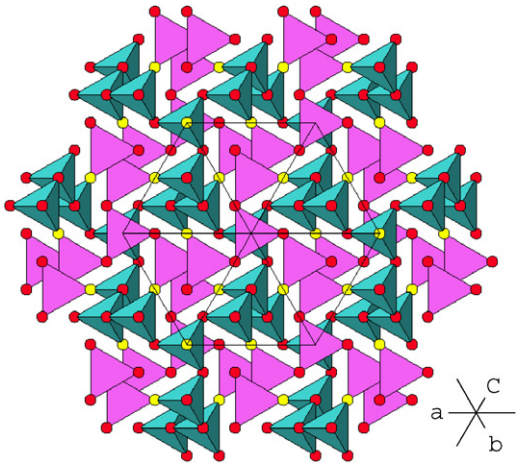

Fig. 4. The [111] projection of the $\square M_4$ CD-core tetrahedra of bixbyite: both subsets, light blue and pink respectively, are shown. The infinite, 3-corner-shared networks of tetrahedra in each subset, spiral around the 3-fold screw axes. The two subsets are linked through the corner-sharing of the fourth tetrahedral vertex, shown in yellow. *Within* each subset, the CD core linkages are $\frac{1}{2}\langle 110\rangle_F$; *between* them, the linkages are $\frac{1}{2}\langle 111\rangle_F$ along all four, equivalent $\langle 111\rangle$ directions of the cubic cell. (The [111] linkage is obscured in this projection).

It follows that three vertices of each $\square M_4$ tetrahedron in each subset are shared with other $\square M_4$ tetrahedra of the same subset. Fig. 4 shows the drawing of the $\square M_4$ tetrahedra of both subsets in the [111] projection, and fully reveals the tetrahedral corner sharing within each, and, additionally, the sharing of the fourth tetrahedral vertex of each tetrahedron in the longer, $\frac{1}{2}\langle 111\rangle_F$ link between the two sets.

We have previously described such links as "in-phase" and "anti-phase" respectively. One consequence of all this is that every cation in the structure is part of a $\square M_4$ CD core. A further consequence is that each peripheral OM_4 tetrahedron of each CD for a given set is common to another CD in that set, and this can be described as CD merging or condensation to produce an infinite CD polymer. However, there is no merging of these peripheral OM_4 tetrahedra from different sets: the $\frac{1}{2}\langle 111\rangle_F$ CD anti-phase links between sets, illustrated in Figs. 2a and b, involve only edge-sharing of OM_4 tetrahedra in each polymer. We have already shown that the overall composition of the CD as defined is $\square M_{4/8}(OM_{4/8})_6$. It follows that the "monomer" of these polymerised CDs has the formula $\square M_{4/8}(OM_{4/8})_3$ or $\square M_2O_3$, each of the $OM_{4/8}$ tetrahedra surrounding the "vacancy" now being shared with another monomer of the same set. The picture which emerges is one where two such discrete, infinite polymers of overall composition M_2O_3, corresponding to the infinite networks of *A*- and *B*-type CDs respectively, share appropriate $OM_{4/8}$ tetrahedral edges (as in Figs. 2a and b) to give the overall structure.

We are grateful to Professor Angel Vegas [private communication] for drawing our attention to the fact that the vacancy net for bixbyite (combining the blue and pink vacancies depicted in Fig. 3) is the same as that for the high-pressure phase of silicon, space group $Ia\bar{3}$ with the Si atoms occupying the 16*c* sites. The same is true, he informs us, for the Si net in the alloy $SrSi_2$. These facts reinforce the underlying unity of inorganic crystal structures, as argued by Hyde and O'Keeffe [35] in their classic 1985 paper.

Again, we note that there are oxides with the bixbyite-type structure which have important applications in the field of optoelectronics: these are the various, doped indium oxides [36–39].

Hoskins and Martin [40], in their analyses, have focussed almost exclusively on the octahedral representation of the CD — the vacancy, coordinated by 6 O atoms. In bixbyite, these

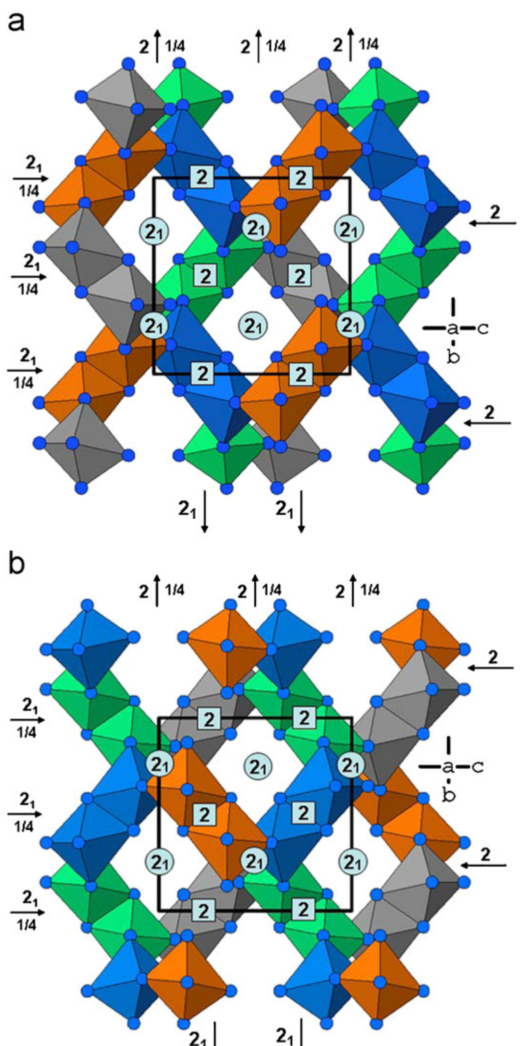

Fig. 5. (a) The infinite network of edge-shared, type-A $\square O_6$ octahedral CD dimers in bixbyite, projected near [100]. The dimers spiral around the 2_1 axes. The heights above the projection plane (*x*-parameters) are distinguished by different colours – 1/8 and 9/8 (grey), 3/8 (green), 5/8 (blue) and 7/8 (orange). (b) The type-B CD dimers of bixbyite as in (a). The patterns are essentially identical but shifted relative to one another.

$\square O_6$ octahedra in any one subset share three edges and all 6 vertices with adjacent $\square O_6$ octahedra, as is shown in Fig. 5: 5a for *A*-type CDs and 5b for *B*-type. It is clear from these drawings that edge-sharing pairs of $\square O_6$ octahedra at one level further share edges with like pairs above and below them, and these CD pairs spiral about the 2_1 axes of the structure. It could be argued that this CD "dimer" constitutes the repeating structural *motif* of bixbyite.

The two types of octahedra are not directly connected as such; their networks just interpenetrate, as Hoskins and Martin concluded previously [40]: the direct network connections occur through the $\frac{1}{2}\langle 111\rangle_F$ links between anti-phase $\square M_4$ tetrahedral CD cores, as already pointed out and shown in Fig. 4.

4.2. Braunite

The braunite structure of manganese silicate, $Mn^{2+}(Mn^{3+})_6SiO_{12}$ was first reported by De Villiers [29] just as a more detailed study by Moore and Araki [30] was submitted for publication. In this, the authors further explored in considerable detail the relationship of the braunite structure to the bixbyite structure in particular and, more generally, to "…*the large family of anion-deficient fluorite derivative structures*". Both studies are in good agreement: however, we focus here on the latter.

The braunite structure is tetragonal, space group $I4_1/acd$, with origin on $\bar{1}$, $a = 9.408$ Å and $c = 18.668$ Å (twice the bixbyite *c*-axis). There are four crystallographically-distinct Mn atoms in Wyckoff sites 8*b* (Mn1), 16*c* (Mn2), 16*e* (Mn3) and 16*f* (Mn4) respectively, and three such oxygen sites, all in 32*g*. Moore and Araki [30] have also described in detail the various cation coordination polyhedra: *"Braunite is based on the packing of cubes (Mn1); octahedra (Mn2, Mn3 and Mn4); and tetrahedra (Si). Excepting the SiO_4 tetrahedron, the polyhedra are substantially distorted away from regular geometry…"*. Comparison is made with those for bixbyite. We now discuss this structure from the CD perspective, and, as did Moore and Araki [30], we compare braunite and bixbyite. From the outset, however, we recognise that this structure can no longer be described in CD terms alone, as with bixbyite: this is because Mn(1) is in cubic coordination with oxygen and cannot be part of a CD core (the $\square M_4$ tetrahedron) since no vacancy exists in its coordination sphere. Nonetheless, we have explored below the CD arrangement in braunite, but, having described in some detail our *modus operandi* in the bixbyite case, we focus here more on the $\square O_6$ octahedra in braunite.

As before, the vacancy sites are obtained by superimposing the ideal fluorite oxygen sites of the unit cell on a drawing of the actual structure and then matching the observed O atom sites to these: the missing match is then the single vacancy site in position 32*g* with coordinates 0.6250, 0.1250, 0.0625. The general cell formula is $M_{64}O_{96}\square_{32}$. Again, we distinguish between the two anion and vacancy subsets.

Fig. 6 shows both types of $\frac{1}{2}\langle 110\rangle_F$ vacancy linkages for this structure, projected near the rather long, unique *c*-axis. It reveals that each vacancy in a given subset is linked to four others (in contrast to the bixbyite case, where this number is three) and the two networks (bixbyite and braunite) are clearly different. Fig. 6 also shows very clearly the columns of $Si\square_4$ tetrahedra, separated by Mn(1) atoms (yellow), which lie on the $\bar{4}$ axes of the space group, the Si atoms (green) being the inversion points

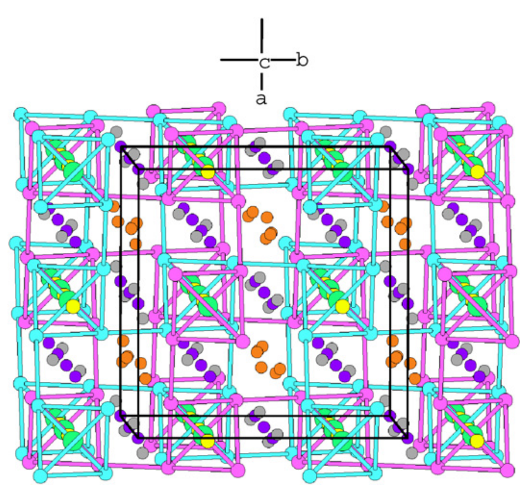

Fig. 6. The two interpenetrating networks of *A*- and *B*-type $\frac{1}{2}<110>_F$ vacancy linkages (light blue and pink respectively) in braunite, projected near the [001] unique axis of the $I4_1/acd$ space group. There are columns of $Si\square_4$ tetrahedra, separated by Mn(1) atoms, along the fourfold inversion axes of the space group (parallel to the *c*-axis), and these columns are cross-linked: the inversion centres for these axes are Si atoms, shown in green. Mn(1) is yellow, Mn(2) purple, Mn(3) grey and Mn(4) brown. Each vacancy is linked to four others.

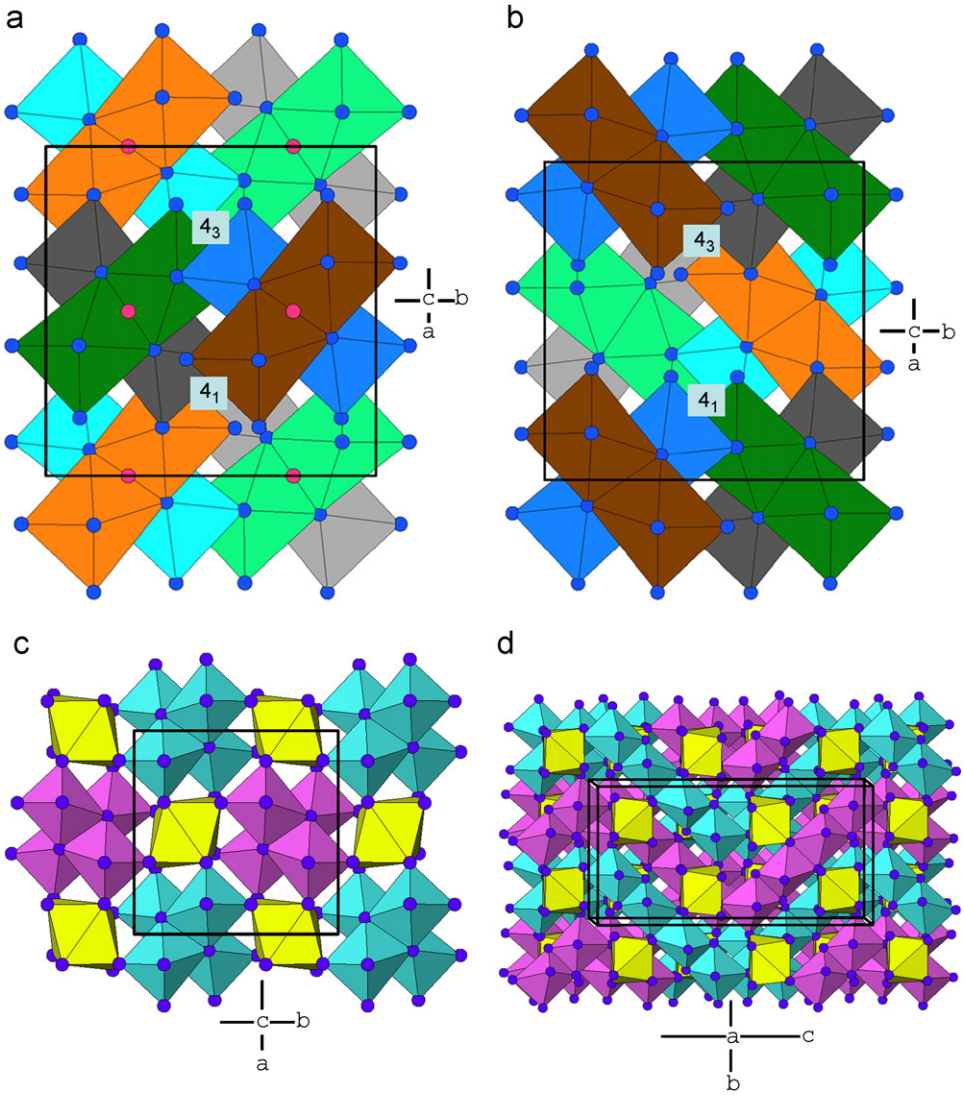

Fig. 7. (a) Braunite clusters of type *A* $\square O_6$ octahedral CDs in the [001] projection. $z = 0.0625$ (light grey), 0.1875 (light green), 0.3125 (light blue), 0.4375 (orange).: $z = 0.5625$ (dark grey), 0.6875 (dark green), 0.8125 (dark blue), 0.9375 (brown). (b) Braunite clusters of type *B* $\square O_6$ octahedral CDs in the [001] projection, as in Fig. 8a. (c) A single (001) slab of braunite clusters centred on $z = 0.375$ projected along [001], showing very clearly how the $Mn(1)O_8$ cubes (yellow) bridge the clusters (type A—light blue; type B—pink). (d) The complete braunite structure projected near [100]. Type A clusters are light blue, type B clusters are pink, bridging $Mn(1)O_8$ cubes are yellow.

for this operation. Thus there exist tetrahedral groupings of four $\square M_4$ tetrahedra, with a central Si atom common to all. This group contains 12 peripheral cations comprising four each of Mn(2), Mn(3) and Mn(4): every one is common to another group, so the overall cation content of the group is $SiMn_6$.

We now translate this situation to the $\square O_6$ octahedra. The tetrahedral group becomes a complex tetrahedron of octahedra, $Si(\square O_6)_4$, derived by the face-sharing of four $\square O_6$ octahedra with the four faces of the central SiO_4 tetrahedron, and each of these contains the inscribed $\square M_4$ tetrahedron. These $Si(\square O_6)_4$ groups alone constitute the CD structure of braunite, and have the same kind of edge-sharing octahedral pairs as in bixbyite, but these pairs are now differently juxtaposed. This is clearly another form of CD merging or polymerisation involving four CDs, and the *motif* in this case we shall call the "braunite cluster". The CD structure of braunite is then two interweaving 3D networks, types *A* and *B*, of edge-sharing clusters The linkage between the two is again effected through the $\frac{1}{2}\langle 111\rangle_F$ anti-phase linkage of $\square M_4$ tetrahedra, but also, as we shall see, through the $Mn(1)O_8$ cubes. Fig. 7a shows *A*-type $\square O_6$ octahedra in the [001] projection at eight levels between $z = 0$ and 1 along the *c*-axis. Fig. 7b shows in similar fashion the arrangement of type *B* CDs. The two sets interweave, and within each set the clusters share edges around the 4-fold screw axes.

These $\square O_6$ octahedra are somewhat distorted, with two short $\square$–O bonds of length ~1.9 Å and four of ~2.2 Å. This inequality simply reflects the distortion of the O lattice from the ideal, and is of no particular significance. The dominant feature of the cluster structure is the Si^{4+} cation at its epicentre. The four $\square M_4$ tetrahedra and four OM_4 tetrahedra which surround the Si atom constitute an element of the sphalerite (ZnS) structure. In isolation, the cluster periphery consists of six pairs of free-standing O atoms, 8 O(1) and 4 O(2), but now, introducing into the total structure the $Mn(1)O_8$ cubes, it transpires that these not only bridge the pairs of peripheral cluster O atoms (Fig. 7c), but, in doing so, they also link clusters of both kinds in all three directions (Fig. 7d). Each $Mn(1)O_8$ cube is surrounded by six clusters, three of each type, and each cluster is surrounded by six $Mn(1)O_8$ cubes, i.e. 1 $Mn(1)O_8$ cube per cluster, and this is the basic structural unit. The complete structure is shown in Fig. 7d, now near the [100] projection. Further examination of Fig. 7d reveals the existence of slabs of these structural units, of both

types *A* and *B*, parallel to (001) and related by the 2_1 screw axes along *b* at $z = \frac{1}{4}, \frac{3}{4}$. A single slab in the [001] projection is shown in Fig. 7c, which demonstrates even more clearly the role of the $Mn(1)O_8$ cubes.

The chemical composition of the structure can now be derived. Within the cluster, the cation content has already been shown to be $SiMn_6$: to this must now be added the one Mn(1) atom associated with each cluster, giving $SiMn_7$. The four O(3) atoms of the SiO_4 tetrahedron are wholly within the cluster, while the eight O(1) atoms in the periphery are those in shared octahedral edges of two clusters and so count as $\frac{1}{2}$. The four O(2) atoms of the cluster are not shared with another cluster and count as 1, yielding the overall composition $SiMn_7O_{12}\square_4$, or $M_2O_3\square$.

Moore and Araki [30] discussed this structure purely in terms of the various cation-centred polyhedra, whereas we have emphasised the structural arrangement of CD octahedra, and in doing so have focussed on the clustering of these. However, the existence of the CD cluster implies also a concomitant clustering of the $\square M_4$ tetrahedra around the central SiO_4 tetrahedron, to which we have referred already (see above). If we now explore the cation-centred polyhedra of the cluster, a most interesting observation emerges. Fig. 8 shows that the twelve peripheral MnO_6 octahedra of the braunite cluster encapsulate the central SiO_4 tetrahedron (green) in an orientation remarkably similar to that of the twelve WO_6 octahedra which cluster around a central PO_4 tetrahedron in the structure of the $[PW_{12}O_{40}]^{3-}$ heteropolyphosphotungstate anion (*cf*., Fig. 145 in Ref. [41]): indeed, the two arrangements are almost identical, suggestive of a heteropolysilicomanganate $[SiMn_6O_{12}]^{2-}$ anion! However, in braunite, each peripheral MnO_6 octahedron is common to an adjacent such cluster (see Fig. 9), so that there is an infinite network of these into which the $Mn(1)O_8$ cubes are intercalated through corner sharing, as shown in Figs. 7c and d.

This braunite structure is a timely reminder that the unit-cell cations of a *fcc* lattice can be depicted in the less-familiar manner illustrated in Fig. 145a of Ref. [41], which emphasises the cuboctahedron with twelve metal atoms located at its vertices and one at its centre. The complete *fcc* lattice is generated through the repeated sharing of the six cuboctahedral square faces with those of the six adjoining cuboctahedra. We have now shown that the braunite anion can be represented as a closed polyhedral group of composition $[Mn_6SiO_{12}]^{2-}$ which, in the overall structure, can be described as a Si-centred cuboctahedron whose twelve vertices are each corner-shared with other Si-centred cuboctahedra, as shown in Fig. 9. The full *fcc* cuboctahedral array is completed by cuboctahedral cavities created by the corner-sharing $Si(Mn)_{12}$ groups and centred by Mn(1) cations (yellow). There are thus equal numbers of Si-centred and Mn(1)-centred cuboctahedra in braunite, the latter not depicted as such in Fig. 9. Nature is indeed very elegant!!

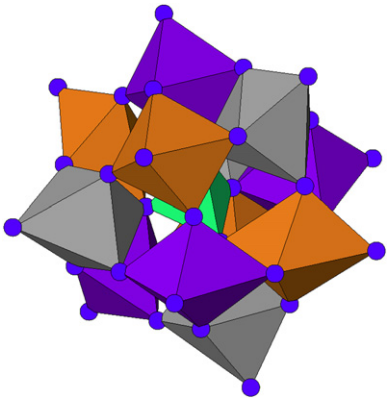

Fig. 8. The cuboctahedral grouping of 12 cation-centred MnO_6 octahedra around the SiO_4 central tetrahedron in braunite: each SiO_4 tetrahedral vertex is shared with 3 MnO_6 octahedral vertices. The overall structure of this grouping mimics that of the $(PW_{12}O_{40})^{3-}$ heteropolyphosphotungstate ion.

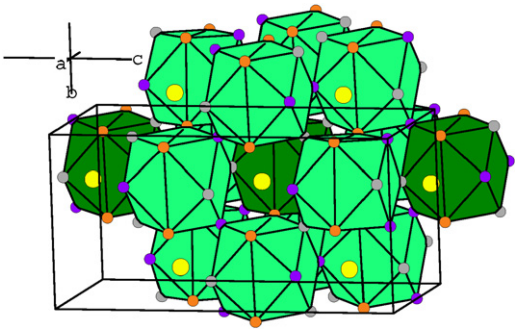

Fig. 9. Si-centred $SiMn_{12}$ cuboctahedra in the polymeric braunite anion. Each of the 12 corners of a central cuboctahedron (dark green) is common to an adjacent cuboctahedtron (light green): $Mn(1)^{2+}$ cations (yellow) centre the cuboctahedral cavities thus created.

4.3. Braunite II

The ideal composition of braunite is $Mn^{2+}(Mn^{3+})_6SiO_{12}$; however, a second polymorph was reported by De Villiers in 1946 [42] termed "*ferrian braunite*" with approximately half the silica content, i.e. $Mn^{2+}(Mn^{3+})_{14}SiO_{24}$. Subsequently De Villiers and Herbstein [31] considered this to be "*an ordered version of ordinary braunite and is provisionally called braunite II*". Braunite II is tetragonal with the space group $I4_1/acd$ and $a = 9.44$ Å, much the same as braunite: however, it differs in that its *c*-axis is doubled to 37.76 Å, *ie*. four times that of bixbyite. This lengthening provided the basis for J.P.R De Villiers' suggestion that braunite II was likely to consist of a braunite cell stacked in a regular manner together with two Mn_2O_3 cells. Finally, the subsequent J.P.R De Villiers' crystal structure determination [32] clearly confirmed the presence of an intergrowth of braunite- and bixbyite-type structures: the sample used had the ideal composition $Ca[(Mn,Fe)_{14}]^{3+}SiO_{24}$. Similar to the role of Mn(1) in braunite, there is one cation, Ca^{2+}, which is coordinated by 8 oxygen atoms in the form of a distorted cube, and so is not part of the underlying CD structure. Indeed, the braunite II structure reinforces our CD interpretation of the braunite structure.

As with braunite, we have first depicted the CD structure and then introduced the CaO_8 cubes into the picture. Because of the doubling of the *c*-axis, there are now two sets of 32*g* vacancy sites, compared with just one set for braunite, and this has interesting consequences. The results are shown in Figs. 10a–c: Fig. 10a shows the whole polyhedral set of types *A* and *B* CDs and CaO_8 cubes: Fig. 10b shows discrete braunite-type slabs parallel to (001) of types *A* and *B* CD clusters bridged by CaO_8 cubes (all the vacancies associated with these clusters occupy only one of these two 32*g* sets). Fig. 10c shows the intervening bixbyite-type slabs linked by the CaO_8 cubes of the braunite-type slabs, although for clarity the CD clusters of these braunite-type slabs have not been depicted: the CD *motifs* of bixbyite, involving exclusively the other vacancy set, are clearly in evidence along the two 2_1 axes of the tetragonal space group, one along *a*, the other along *b*.

4.4. Parwelite

We now finally turn our attention to the even more chemically complex mineral, parwelite, whose idealised composition is $(Mn^{2+})_{10}Sb_2As_2Si_2O_{24}$. Its existence in Sweden was reported

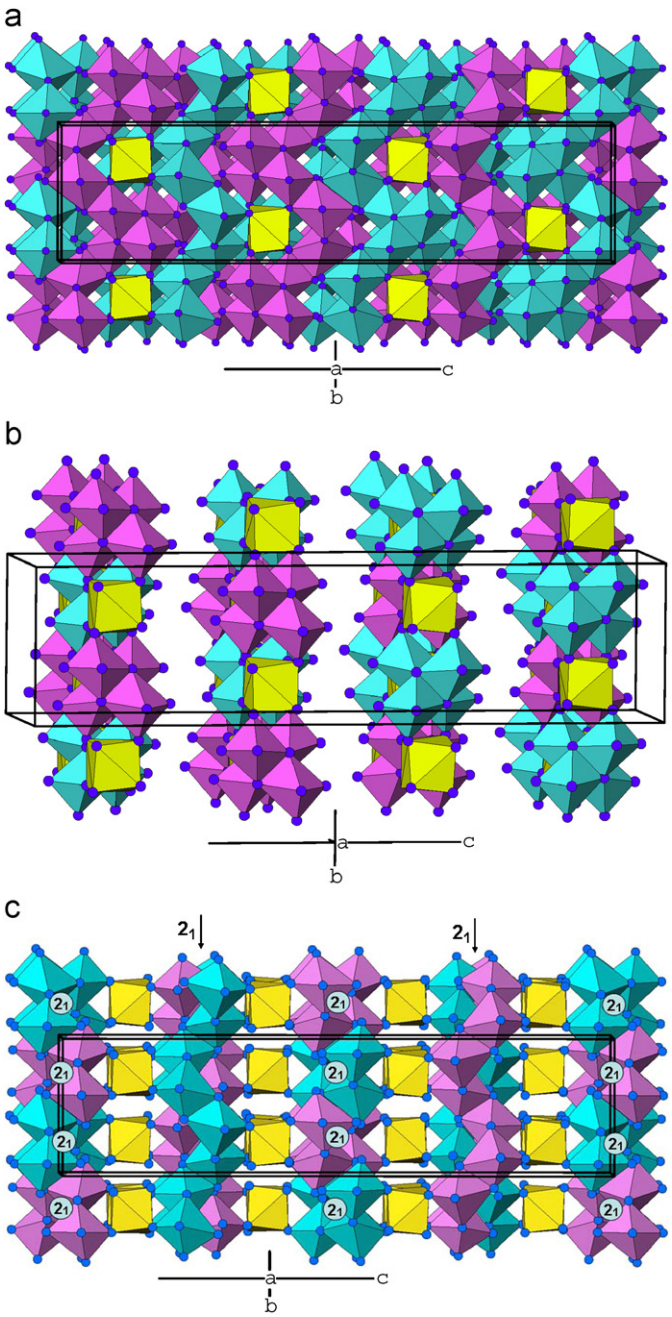

Fig. 10. (a) Full CD detail for Braunite II: discrete (001) slabs of braunite-type clusters separated by parallel bixbyite-type slabs, and all linked together by intercalated CaO_8 cubes (yellow). (b) Braunite II. Discrete slabs of braunite-type clusters linked by CaO_8 cubes. Intervening slabs of bixbyite-type structure are not shown in this drawing. (c) Braunite II. Bixbyite-type (001) slabs, centred on the labelled 2_1 axes, are linked by the CaO_8 cubes (yellow) of the braunite-type slabs whose CD clusters are not shown in this drawing.

originally by Moore [43] and its structure determined (a *tour de force*) subsequently by Moore and Araki [23]. It is monoclinic, with $a = 10.048$ Å, $b = 19.418$ Å, $c = 9.735$ Å and $\beta = 95.83°$. Their attempted refinement in the centrosymmetric space group $A12/a1$ was unsuccessful, but a satisfactory result was achieved with the non-centrosymmetric group Aa. These authors give a comprehensive analysis of the structure in group-theoretical terms, following a similar, earlier analysis of the braunite structure, and their emphasis is again on the cation-centred polyhedra.

In a later paper, Marsh and Schomacher [44] demonstrated that, with the same data and a shift of origin, successful refinement could be achieved in space group $A12/a1$. There is little difference between the two results, and we have used the centrosymmetric structure in what follows, where again we emphasise the role of the octahedral CDs. (Even in this centrosymmetric structure, there are still 8 crystallographically distinct cations, 12 such oxygen atoms and four vacancies, highlighting just how formidable was the task facing Moore and Araki using the non-centric space group!)

Again, we recognise that this structure cannot be described in CD terms alone because $M(7)$ is in cubic coordination with oxygen and cannot be part of a CD core. (Indeed, the parwelite ideal composition can also be represented as the "salt" $Mn^{2+}[(Mn_4)^{2+}As^{5+}Sb^{5+}Si^{4+}O_{12}]^{2-}$.) But now the assignment of the vacancy sites is not quite so straightforward as in the other cases. This problem arises because of the considerable displacement of some O atoms from their ideal positions, particularly in the region between neighbouring As and Si atoms. Nevertheless, given the reported structure, there is only one sensible assignment possible, and this we have used in our analysis.

The short, $\frac{1}{2}\langle 110\rangle_F$ CD links between types A and B vacancies, unlike the bixbyite and braunite cases, occur in parwelite as discrete, infinite slabs parallel to (010), and *within* these slabs some vacancies are linked to four others, some to three. This is shown in Fig. 11, near the [100] projection, and implies that *within* each slab there are some metal atoms which are common to four $\square M_4$ tetrahedra, others to three, while the linkages *between* slabs are again through anti-phase, $\frac{1}{2}\langle 111\rangle_F$ linkages involving edge-sharing between the OM_4 tetrahedra of each CD type. We now explore the slab structure in greater detail.

Fig. 12a shows these slabs as CDs, depicted as $\square O_6$ octahedra, in the same projection, and it is clear that the octahedra are somewhat more distorted than those in braunite, for instance. Of more significance is Fig. 12b, which shows an A-type slab of CDs (typical of all such slabs) in the [010] projection. Clearly visible are $(\square O_6)_4$ clusters (dark blue), as in braunite, but here they are discrete. They are connected, however, through bixbyite-type CD spirals (light blue). But, here it is the $M(6)$ cation at the centre of these clusters, in a very distorted octahedral environment (4 O atoms at ~2.06 Å, another 2 at 2.88 Å), rather than SiO_4 tetrahedra, as in the two braunites. Moreover, in this structure, the Si coordination is 4 O atoms at the normal distance of ~1.6 Å, with a fifth at a much greater distance (2.95 Å), and only three vacancies rather than the expected four, as in the two braunites.

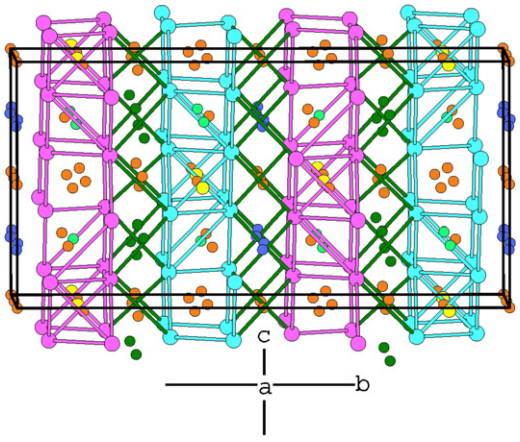

Fig. 11. Parwelite. (010) slabs of type A (light blue) and type B (pink) $\frac{1}{2}\langle 110\rangle_F$ vacancy linkages near the [100] projection. These slabs are cross-linked by $\frac{1}{2}\langle 111\rangle_F$ anti-phase CD linkages (dark green).

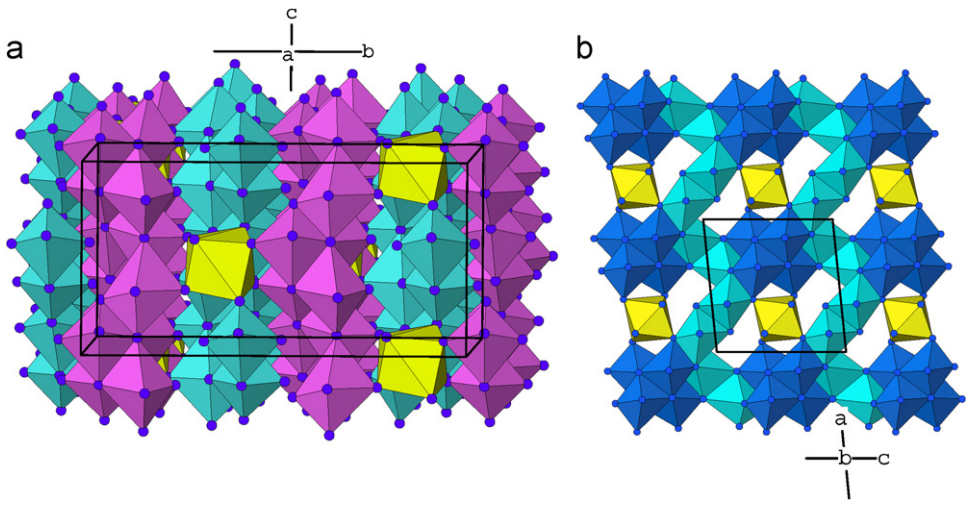

Fig. 12. (a) Parwelite. A projection near [100] of the (010) slabs of type A (light blue) and type B (pink) $\square O_6$ octahedral CDs cross linked by $M(7)O_8$ cubes (yellow). (b) Parwelite. A [010] projection of a single *A*-type slab centred on $y = 0.375$ showing discrete braunite-type clusters (dark blue) linked by bixbyite-type CD spirals (light blue and all cross-linked by $M(7)O_8$ cubes (yellow).

In the light of these unexpected anomalies, we have therefore decided to seek confirmation of the reported structure before proceeding further.

5. Conclusion

Despite the increasing complexity of these structures, there are clear and defining relationships, not only in the cation layers (as emphasised by Moore and Araki), but also from the viewpoint of the distribution of CDs, as explored above. The cation contents, however, are very different in the structures discussed here; a single cation species in bixbyite, two in braunite and four in parwelite.

In the paper by Moore and Araki [23] describing the structure of parwelite, they make this statement: "*The problem then reduces to inquiring how these vacancies are ordered and then inquiring about the coordination number for the cations* ***as a consequence of this ordering*** (our emphasis)". To the contrary, we would assert that the arrangement of the vacancies in the multi-cation compounds is not only the result of *the actual cations present, the sites they occupy and their coordination preferences, but also of the structure-determining topology of the octahedral CDs*.

Finally, for this whole group of minerals, the recognition in the braunite structure of the significance of the Si-centred cuboctahedra and their juxtaposition leads us to comment on this aspect of the bixbyite and parwelite structures. In bixbyite, there is, of course, no Si, just two sets of Mn atoms: (Mn(1) in the 8*a* site of $Ia\bar{3}$ and Mn(2) in the 24*d* site. In cuboctahedral terms, the structure has $Mn(1)Mn(2)_{12}$ cuboctahedra, each sharing six square faces, as in the complete *fcc* lattice, the central polyhedron being a $Mn(1)O_6$ grouping. The intergrowth structure of braunite II means that (001) slabs of braunite-type cuboctahedra alternate with (001) slabs of bixbyite-type cuboctahedra, all sharing square faces. In parwelite, the reported cation sites give rise to a structure in which pairs of Si-centred cuboctahedra, joined at a square face, are interspersed with like pairs of Mn(5)-centred cuboctahedra to generate the full *fcc* cuboctahedral array.

Although interesting in itself, the cuboctahedral description of these structures ignores completely the anion sub-lattice, whereas our CD approach, in contrast, while not ignoring the cations, emphasises the important, structure-determining role that is also played by the anions, both present and missing, in these ubiquitous fluorite-related oxides.

Acknowledgments

These authors wish to place on record their gratitude to their respective progeny, Mr. Andrew Bevan and Dr. Lisa Martin for their considerable help with the modern computer technology inherent in present-day publishing. We also acknowledge the help accorded by Dr. Eric Dowty, of Space Software in adapting his ATOMS program to our special drawing needs, for scientific input from Drs Max R. Taylor and Sharon E. Ness, and for discussions with Professors Strähle and Hoppe.

Finally, we pay tribute to our dear friend and colleague, the late Dr. B.F. Hoskins.

References

[1] D.J.M. Bevan, W.W. Barker, R.L. Martin, Rare Earth Research, Gordon & Breach, New York, 1965, pp. 441–460.
[2] T.C. Parks, D.J.M. Bevan, Revue de Chimie Minérale 10 (1973) 15.
[3] D.J.M. Bevan, E. Summerville, in: K.A. Gschneider Jr., L. Eyring (Eds.), Handbook of Physics and Chemistry of the Rare-earths, Vol. 3, North Holland, 1979, pp. 401–524.
[4] B.F. Hoskins, R.L. Martin, D.J. Taylor, J. Chem. Soc. (1978) 320–328.
[5] R.L. Martin, Nature 165 (1950) 202–203.
[6] W. Schottky, C. Wagner, Z. Phys. Chem. B 11 (1930) 163.
[7] B.G. Hyde, D.J.M. Bevan, L. Eyring, Phil. Trans. Roy. Soc. London A 259 (1966) 583–614.
[8] D.J.M. Bevan, J. Inorg. Nucl. Chem. 1 (1955) 49–56.
[9] S.F. Bartram, Inorg. Chem. 5 (1966) 749–754.
[10] M.R. Thornber, D.J.M. Bevan, J. Graham, Acta Cryst. B 24 (1968) 1183–1190.
[11] M.R. Thornber, D.J.M. Bevan, J. Solid State Chem. 1 (1970) 536–544.
[12] J.G. Allpress, H.J. Rossell, H.G. Scott, Mater. Res. Bull. 9 (1974) 455–468.
[13] L. Eyring, in: K.A. Gschneider Jr., L. Eyring (Eds.), Handbook of Physics and Chemistry of the Rare-earths, Vol. 3, North Holland, 1979, pp. 337–399.
[14] Z.C. Kang, L. Eyring, Aust. J. Chem. 49 (1997) 981–996.
[15] R.B. Von Dreele, L. Eyring, A.L. Bowman, J.L. Yarnell, Acta Cryst. B 31 (1975) 971–974.
[16] J. Zang, R.B. Von Dreele, L. Eyring, J. Solid State Chem. 104 (1993) 21–32.
[17] J. Zang, R.B. Von Dreele, L. Eyring, J. Solid State Chem. 118 (1995) 133–140.
[18] J. Zang, R.B. Von Dreele, L. Eyring, J. Solid State Chem. 118 (1995) 141–147.
[19] J. Zang, R.B. Von Dreele, L. Eyring, J. Solid State Chem. 122 (1996) 53–58.
[20] D.J.M. Bevan, R.L. Martin, Z. Anorg. Allg. Chem. 625 (1999) 57–69.
[21] B.F. Hoskins, R.L. Martin, Aust. J. Chem. 48 (1995) 709–739.
[22] R.L. Martin, J. Chem. Soc. Dalton Trans. (1997) 3659–3670.
[23] P.B. Moore, T. Araki, Inorg. Chem. 16 (1977) 1839–1847.
[24] R.L. Martin, J. Chem. Soc. Dalton (1974) 1335–1350.

[25] A.D. Wadsley, S. Andersson, Perspect. Struct. Chem. (1970) 1.
[26] B.F. Hoskins, R.L. Martin, J. Chem. Soc. (1976) 676–685.
[27] J. Choisnet, L. Bizo, R. Retoux, B. Raveau, J. Solid State Chem. 177 (2004) 3748–3751.
[28] P.B. Moore, Mineral. Record (Winter) (1971) 154–172.
[29] J.P.R. De Villiers, Am. Mineral. 60 (1975) 1098–1104.
[30] P.B. Moore, T. Araki, Am. Mineral. 61 (1976) 1226–1240.
[31] J.P.R. De Villiers, F.H. Herbstein, Am. Mineral. 52 (1967) 20–30.
[32] J.P.R. De Villiers, Am. Mineral. 65 (1980) 756–765.
[33] L.D. Pauling, M.D. Shapell, Z. Krist. 75 (1930) 128.
[34] S. Geller, Acta Cryst. B 27 (1971) 821–828.
[35] M. O'Keeffe, B.G. Hyde, Struct. Bond. 61 (1985) 77–144.
[36] G. Franck, H. Köstlin, Appl. Phys. A 27 (1982) 197.
[37] J. Choisnet, L. Bizo, R. Retoux. B. Raveau, Solid State Sci. 6 (2004) 1121–1123.
[38] L. Bizo, J. Choisnet, R. Retoux, B. Raveau, Solid State Commun. 136 (2005) 163–168.
[39] L. Bizo, J. Choisnet, B. Raveau, Mat. Res. Bull. 41 (2006) 2232–2237.
[40] B.F. Hoskins, R.L. Martin, J. Chem. Soc. 24 (1975) 576–588.
[41] A.F.W. Wells, Structural Inorganic Chemistry, 3rd ed., Oxford University Press, 1962, pp. 448–452.
[42] J.E. De Villiers, Trans. Geol. Soc. South Africa 48 (1945) 17–26.
[43] P.B. Moore, Arkiv foer Mineralogi och Geologi 4 (1968) 467–472.
[44] R.E. Marsh, V. Schomacher, Inorg. Chem. 18 (1979) 2331–2336.